processes

MDPI

Article

Study of Torsional Vibration Bifurcation Characteristics of Direct-Drive Wind Turbine Shaft System

Zhonghua Huang [1], Rongjie Wu [1], Jinhao Chen [1], Xin Xu [2] and Ya Xie [1,*]

[1] College of Mechanical Engineering, Hunan Institute of Engineering, Xiangtan 411100, China
[2] Harbin Electric Corporation Wind Power Co., Ltd., Xiangtan 411100, China
* Correspondence: yxie@hnie.edu.cn

Abstract: This paper set out to establish the dynamics model of shaft torsional vibration for direct-drive wind turbine with the phenomenon of unstable shaft system torsional vibration. The stability of the equilibrium point of the dynamical model is investigated, and the Routh–Hurwitz stability criterion is used to obtain a range of values for the bifurcation control parameters. For the stable equilibrium point, the stability domain of the system is calculated by constructing the Lyapunov function. The sensitivity analysis of system parameters is carried out to obtain the law of the effect of system parameters on system stability of the torsional vibration system. The results are substituted for example calculations, and the results verify the correctness of the theoretical analysis conclusions. It is proved that it is feasible to analyze the torsional vibration characteristics of the direct-drive wind turbine shaft system by using the principle of Routh–Hurwitz stability, etc., which provides a reference for the structural design of direct-drive wind turbine.

Keywords: axial torsional vibration; equilibrium point; Hopf bifurcation; stability domain

Citation: Huang, Z.; Wu, R.; Chen, J.; Xu, X.; Xie, Y. Study of Torsional Vibration Bifurcation Characteristics of Direct-Drive Wind Turbine Shaft System. *Processes* **2022**, *10*, 1700. https://doi.org/10.3390/pr10091700

Academic Editors: Krzysztof Rogowski and Zhiwei Gao

Received: 27 June 2022
Accepted: 22 August 2022
Published: 26 August 2022

1. Introduction

Wind power and other new energy sources are developing rapidly and have become the main body of renewable energy development [1]. As one of the types of new energy, the installed capacity of wind turbines maintains a high growth rate in 2020. By the end of 2020, China's power supply had an additional installed capacity of 190.87 million kilowatts, and the cumulative installed capacity of wind power exceeded 280 million kilowatts [2].

Accidents caused by torsional vibration of the wind turbine occasionally occur, threatening the safe and stable operation of the wind turbine. When torsional nonlinear vibration occurs in the shaft system of the direct-drive wind wheel, on the one hand, it will reduce the inherent frequency of the shaft system vibration, which will easily trigger the low-frequency resonance of the shaft system and other parts of the wind turbine and the power grid, and, on the other hand, it can reduce the stability of the shaft system vibration and can easily trigger shaft system oscillation instability [3,4].

In order to improve the reliability of wind turbines during operation, the available literature shows that it is possible to analyze the factors that generate failures in wind turbines or the stability of vibration phenomena. For example, the literature [5] provides a review of existing fault diagnosis, prediction, and resilience control methods and techniques for wind turbine systems. The literature [6] investigates data-driven fault diagnosis and fault classification strategies for wind energy systems under various fault scenarios. For the phenomenon of torsional vibration of the wind turbine shaft system, its nonlinear vibration is, generally, analyzed. For example, the literature [7] establishes an electromechanical small signal model of a doubly-fed wind wheel applicable to the analysis of the dynamic characteristics of the shaft system, and carries out the analysis of the torsional vibration mechanism and the design of the suppression strategy based on this model. In the literature [8], a mathematical model of a direct-drive permanent magnet synchronous

wind wheel was established, including wind wheel, drive train, motor, and grid, and a nonlinear control strategy for coordinated control was proposed.

Currently, there are more studies on wind turbine stability, such as literature [9] which proposed a control stability analysis of cross-axis wind turbine pitch system based on the Kharitonov robust stability method to evaluate the robust stability of the pitch controller. The literature [10] proposes single and combined automatic reactive power support (ARS) control techniques for renewable energy sources to improve system stability by injecting available reactive power into the system through converters during faults.

Parametric effect analysis or sensitivity analysis can analyze the influence characteristics of each design parameter on the stability of the vibration system, according to the literature [11]. The flow through small horizontal axis wind turbines (HAWT) was simulated by hydrodynamics (CFD) simulations, and the effect on the performance of small-scale horizontal axis wind turbines was studied through parametric analysis of fluid dynamics (CFD) simulations, according to the literature [12]. Design evaluation was conducted into Savonius wind turbines (SWTs) by changing system parameters, such as rotor diameter, rotor height, and torsional angle, for urban applications by using transient computational fluid dynamics (CFD) methods. Parametric sensitivity analysis of rotor angular stability indicators for power systems has been analyzed in the literature [13]. The rotor angle stability analysis indexes, such as key fault clearance time (CCT), characteristic value point, damping ratio, frequency deviation, voltage deviation, and generator speed deviation, are identified and analyzed. The results show that if the inertia of any part of the multi-machine power system decreases, the CCT of each component decreases. In the literature [14], local sensitivity analysis was used to establish the relationship between different types of drivetrain faults and system dynamic characteristics and torsional response amplitude. Abnormal deviations in stiffness and moment of inertia due to faults lead to large changes in natural frequency and modal response, which can be measured and used as fault-detection features using the proposed analysis methods.

In this article, we establish the dynamics model of shaft torsional vibration for direct-drive wind turbine with the phenomenon of unstable shaft system torsional vibration. Based on the Routh–Hurwitz stability theorem to analyze the range of values of control parameters when the system is stable and generates a bifurcation phenomenon, the Lyapunov stability theorem reveals the stability domain of the system, and the sensitivity analysis obtains the action law of parameters on the stability of the system in a torsional vibration system. It provides a reference for the structural design of direct-drive permanent magnet wind turbines.

2. Wind Wheel Shaft System Model

The equivalent concentrated mass method is generally used to study the dynamics of the wind turbine shaft system. In the literature [15], a three-mass block shaft system equivalent model was established to analyze the wind wheel torsional vibration mechanism. This article uses an equivalent two-mass block model, as shown in Figure 1, equating the wind wheel as a whole to a mass disc and the generator rotor to another mass disc, and simulating the drive shaft with a massless spring damper.

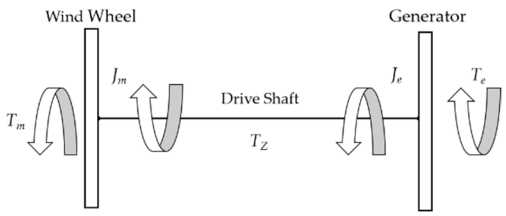

Figure 1. Equivalent mechanical model of the shaft system.

The torsional vibration equation for the shaft system is established as follows:

$$\left.\begin{array}{l} J_m\ddot{\theta} + C_m\dot{\theta} + C_Z\dot{\theta}_Z + K_Z\theta_Z = T_m \\ J_e\ddot{\delta} + C_e\dot{\delta} - C_Z\dot{\theta}_Z - K_Z\theta_Z = -T_e \\ \theta - \delta = \theta_Z \end{array}\right\} \quad (1)$$

The parameters represented by each character are shown in Table 1.

Table 1. Table of values for each parameter.

Characters	Parameters Represented
J_m	Rotational inertia of wind wheel
J_e	Rotational inertia of the generator rotor
K_z	Stiffness coefficient of the drive shaft
C_m	Damping factor of wind wheel
C_e	Damping factor of generator rotor
C_z	Damping factor between wind wheel and generator
T_m	Output torque of wind turbine
θ	Wind turbine rotation angle
δ	Rotation angle of generator rotor
θ_z	Relative torsion angle at both ends of the shaft
T_e	Output torque of the generator

The various symbols in the article and the definitions of the symbols are shown in Table 2.

Table 2. Values for each parameter.

Symbols	Symbol Definition
T_e, T_0	Output torque of the generator
T, T_2	Bifurcation parameters
A_1, A_2	Equilibrium points
$\boldsymbol{H_1}$, $\boldsymbol{H_2}$	Jacobian matrix
$q_{1,2,3,4}$	Polynomial coefficients
Δ_l	Hurwitz determinants
A, B, C	The coefficient of a univariate quadratic polynomial of T_2
R_1, R_2	The roots of the quadratic equation of T_2
u_1, u_2, $\hat{u}_1$, $\hat{u}_2$	Wind turbine rotation angle
δ_1, δ_2, $\hat{\delta}_1$, $\hat{\delta}_2$	Rotation angle of generator rotor
$V(\boldsymbol{x})$	Quadratic function
$\boldsymbol{P}$	Symmetric positive definite matrix
$L(\boldsymbol{x})$	The derivative of $V(\boldsymbol{x})$ with respect to time
ξ	Constant
D	The maximum eigenvalue of $\boldsymbol{P}$
U	Stability domain of the system

Set T_m as a constant and $T_e = T_0 \sin\delta$, Equation (1) is transformed into the following form:

$$\left.\begin{array}{l} J_m\ddot{\theta} + C_m\dot{\theta} + C_Z\left(\dot{\theta} - \dot{\delta}\right) + K_Z(\theta - \delta) = T_m \\ J_e\ddot{\delta} + C_e\dot{\delta} - C_Z\left(\dot{\theta} - \dot{\delta}\right) - K_Z(\theta - \delta) = -T_0\sin\delta \end{array}\right\} \quad (2)$$

Set $u_1 = \theta$, $u_2 = \dot{\theta}$, $\delta_1 = \delta$, and $\delta_2 = \dot{\delta}$. The original Equation (2) is reduced to an equivalent system of first-order state equations, as shown below:

$$\left.\begin{array}{l} \dot{u}_1 = u_2 \\ \dot{u}_2 = \frac{1}{J_m}[-K_Z u_1 - (C_m + C_Z)u_2 + K_Z\delta_1 + C_Z\delta_2 + T_m] \\ \dot{\delta}_1 = \delta_2 \\ \dot{\delta}_2 = \frac{1}{J_e}[K_Z u_1 + C_Z u_2 - K_Z\delta_1 - (C_e + C_Z)\delta_2 - T_0 \sin\delta_1] \end{array}\right\} \tag{3}$$

In Equation (3), T is set as the bifurcation parameter, and the value is T_0/J_e. Let the set of equations be equal to 0. Calculate the equilibrium points A_1, and A_2 of the system as follows:

$$A_1 = (\sin^{-1}\frac{T_m}{TJ_e} + \frac{T_m}{K_z} + 2k\pi, 0, \sin^{-1}\frac{T_m}{TJ_e} + 2k\pi, 0) \tag{4}$$

$$A_2 = (\pi - \sin^{-1}\frac{T_m}{TJ_e} + \frac{T_m}{K_z} + 2k\pi, 0, \pi - \sin^{-1}\frac{T_m}{TJ_e} + 2k\pi, 0) \tag{5}$$

Of the above two points, k = 0, ±1, ±2, ±3, . . . , the values of A_1 and A_2 can be abbreviated as: $A_i = (u_{1i}, u_{2i}, \delta_{1i}, \delta_{2i})$, i = 1, 2.

The state Equation (3) can be transformed into the following matrix form:

$$\begin{bmatrix} \frac{du_1}{dt} \\ \frac{du_2}{dt} \\ \frac{d\delta_1}{dt} \\ \frac{d\delta_2}{dt} \end{bmatrix} = \begin{bmatrix} 0 & u_2 & 0 & 0 \\ -\frac{K_Z}{J_m} & -\frac{(C_m+C_Z)}{J_m} & \frac{K_Z}{J_m} & \frac{C_Z}{J_m} \\ 0 & 0 & 0 & \delta_2 \\ \frac{K_Z}{J_e} & \frac{C_Z}{J_e} & -\frac{K_Z}{J_e} & -\frac{(C_e+C_Z)}{J_e} \end{bmatrix} \begin{bmatrix} u_1 \\ u_2 \\ \delta_1 \\ \delta_2 \end{bmatrix} + \begin{bmatrix} 0 \\ \frac{T_m}{J_m} \\ 0 \\ T\sin\delta_1 \end{bmatrix} \tag{6}$$

Simplifying Equation (6), the first order partial derivatives of the system of equations with respect to the parameters u_1, u_2, δ_1, and δ_2 are found and arranged to obtain the Jacobian matrix $\boldsymbol{H}_1$ of the system as follows:

$$\boldsymbol{H}_1 = \begin{bmatrix} 0 & 1 & 0 & 0 \\ -\frac{K_Z}{J_m} & -\frac{C_m+C_Z}{J_m} & \frac{K_Z}{J_m} & \frac{C_Z}{J_m} \\ 0 & 0 & 0 & 1 \\ \frac{K_Z}{J_e} & \frac{C_Z}{J_e} & -\left(\frac{K_Z}{J_e} + T\cos\delta_1\right) & -\frac{C_e+C_Z}{J_e} \end{bmatrix} \tag{7}$$

The values of the determinant of the matrix $\boldsymbol{H}_1$ are

$$\det\boldsymbol{H}_1 = \frac{K_Z}{J_m} T\cos\delta_1 \tag{8}$$

Substituting the expression of δ_{1i} in points A_1 and A_2 into Equation (8), the cosine value is obtained as follows:

$$\cos\delta_{1j} = (-1)^{j-1}\sqrt{1 - \left(\frac{T_m}{TJ_e}\right)^2} \tag{9}$$

By substituting the bifurcation parameter T into the cosine of the determinant value of the system matrix, the relationship between the bifurcation parameter T and the determinant can be obtained, as shown below:

$$T\cos\delta_{1j} = (-1)^{j-1}\sqrt{T^2 - \left(\frac{T_m}{J_e}\right)^2}, = 1, 2 \tag{10}$$

From the definition of the root formula, it can be seen that: T and T_m/J_e are positive numbers. Further, when $T > T_m/J_e$, there exist two equilibrium points, A_1 and A_2, of the

system; when $T = T_m/J_e$, the equilibrium point A_1 coincides with the equilibrium point A_2; when $T < T_m/J_e$, there is no equilibrium point of the system.

3. Stability Analysis

Analyze the stability of the system at the equilibrium point when $T > T_m/J_e$.

(1) The stability of the equilibrium point A_1 is analyzed by substituting the value of the point A_1 into the determinant of the matrix $\boldsymbol{H}_1$.

$$\det \boldsymbol{H}_1\big|_{A_1} = \frac{K_Z}{J_m} T \cos\delta_{11} = \frac{K_Z}{J_m}\sqrt{T^2 - \left(\frac{T_m}{J_e}\right)^2} > 0 \tag{11}$$

To facilitate the calculation, set

$$T_2 = T\cos\delta_{11} = \sqrt{T^2 - \left(\frac{T_m}{J_e}\right)^2} \tag{12}$$

Equation (3). The Jacobian matrix $\boldsymbol{H}_2$ at the equilibrium point A_1 is:

$$\boldsymbol{H}_2 = \begin{bmatrix} 0 & 1 & 0 & 0 \\ -\frac{K_Z}{J_m} & -\frac{C_m+C_Z}{J_m} & \frac{K_Z}{J_m} & \frac{C_Z}{J_m} \\ 0 & 0 & 0 & 1 \\ \frac{K_Z}{J_e} & \frac{C_Z}{J_e} & -\left(\frac{K_Z}{J_e}+T_2\right) & -\frac{C_e+C_Z}{J_e} \end{bmatrix} \tag{13}$$

The characteristic polynomial of the matrix is:

$$f(\lambda) = \det(\lambda \boldsymbol{E} - \boldsymbol{H}_2) = q_4\lambda^4 + q_3\lambda^3 + q_2\lambda^2 + q_1\lambda + q_0 \tag{14}$$

The coefficients and constant terms of the polynomial are:

$$\left.\begin{array}{l} q_0 = \frac{K_Z T_2}{J_m} \\ q_1 = \frac{K_Z(C_m+C_e)}{J_e J_m} + \frac{C_m+C_Z}{J_m} T_2 \\ q_2 = \frac{C_e C_m + C_e C_Z + C_m C_Z + K_Z(J_e+J_m)}{J_e J_m} + T_2 \\ q_3 = \frac{C_m+C_Z}{J_m} + \frac{C_e+C_Z}{J_e} \\ q_4 = 1 \end{array}\right\} \tag{15}$$

$\boldsymbol{E}$ is a fourth order unit matrix.

Determining the stability of point A_1 by using the Routh–Hurwitz stability criterion [16]. The condition for the stability of the system at point A_1 is whether the Hurwitz determinant of each order is greater than zero Δ_l (l = 1,2,3,4) when $q_4 > 0$ in the eigen polynomial. The specific expressions for each parameter are as follows:

$$\left.\begin{array}{l} q_4 > 0 \\ \Delta_1 = q_3 > 0 \\ \Delta_2 = \det\begin{bmatrix} q_3 & q_4 \\ q_1 & q_2 \end{bmatrix} > 0 \\ \Delta_3 = \det\begin{bmatrix} q_3 & q_4 & 0 \\ q_1 & q_2 & q_3 \\ 0 & q_0 & q_1 \end{bmatrix} > 0 \\ \Delta_4 = \det\begin{bmatrix} q_3 & q_4 & 0 & 0 \\ q_1 & q_2 & q_3 & q_4 \\ 0 & q_0 & q_1 & q_2 \\ 0 & 0 & 0 & q_0 \end{bmatrix} = q_0\Delta_3 > 0 \end{array}\right\} \tag{16}$$

when J_m, J_e, K_z, C_m, C_e, C_z, and T_m are positive, the system Hurwitz determinant $\Delta_1 > 0$, $\Delta_2 > 0$, Δ_3, and Δ_4 have the same symbol, only the symbol of Δ_3 needs to be determined.

Determine the sign of the discriminant Δ_3, Δ_3 can be viewed as a quadratic polynomial with respect to T_2 ($T_2 > 0$)

$$AT_2^2 + BT_2 + C \tag{17}$$

The quadratic coefficient A is:

$$A = \frac{(C_z^2 + C_eC_m + C_eC_z + C_mC_z)}{(J_eJ_m)} \tag{18}$$

Since the parameters J_m, J_e, K_z, C_m, C_e, C_z, and T_m are positive, the coefficient A is constant positive. From the definition of a unary quadratic polynomial, it can be seen that the image opening of Equation (17) is upward, and, when it is greater than zero, the value equivalent to Δ_3 is greater than zero, and the system is stable.

By making Equation (17) equal to zero, the two roots of the polynomial, R_1 and R_2 ($R_1 \leq R_2$), are calculated. Since the value of the bifurcation parameter T is greater than the fixed value T_m/J_e, that is, $T_2 > T_m/J_e\text{co}\delta_{11}$, the value of the two roots compares with the size of the fixed value $T_m/J_e\text{co}\delta_{11}$ in three cases: $R_2 \leq T_m/J_e\text{co}\delta_{11}$, $R_1 \leq T_m/J_e\text{co}\delta_{11} < R_2$, and $R_1 > T_m/J_e\text{co}\delta_{11}$. Under this premise, when T_2 meets the following conditions, the value of Δ_3 is equal to zero.

$$\left.\begin{array}{ll} T_2 > \frac{T_m}{J_e}\cos\delta_{11} \text{and } T_2 = R_1, & R_1 = R_2 \\ \text{None} & R_2 \leq \frac{T_m}{J_e}\cos\delta_{11} \\ R_2 & R_1 \leq \frac{T_m}{J_e}\cos\delta_{11} < R_2 \\ R_1 \text{and} R_2 & R_1 > \frac{T_m}{J_e}\cos\delta_{11} \end{array}\right\} \tag{19}$$

If the matrix $\boldsymbol{H}_2$ has a pair of pure virtual roots $\lambda_{1,2}$ with zero real parts, the remaining characteristic roots $\lambda_{3,4}$ have negative real parts, and the derivative of the real part of the characteristic root λ_1 with respect to the bifurcation parameter T at T_2 is not equal to zero, as shown in Equation (20):

$$\left.\begin{array}{c} Re(\lambda_{1,2}(T))\big|_{T=T_2} = 0 \\ Re(\lambda_{3,4}(T))\big|_{T=T_2} < 0 \\ Re(\lambda'(T))\big|_{T=T_2} \neq 0 \end{array}\right\} \tag{20}$$

According to the high-dimensional Hopf bifurcation theory, when the bifurcation parameter T satisfies Equations (19) and (20), the system generates a Hopf bifurcation at the equilibrium point A_1.

Since T_2 satisfies Equation (19), the value of Δ_3 is equal to zero, further, when T_2 satisfies the following conditions, the discriminant $\Delta_3 > 0$, $\Delta_4 > 0$, and the system is stable.

$$\left.\begin{array}{ll} T_2 > \frac{T_m}{J_e}\cos\delta_{11}, T_2 \neq R_1 & R_1 = R_2 \\ T_2 > \frac{T_m}{J_e}\cos\delta_{11} & R_2 < \frac{T_m}{J_e}\cos\delta_{11} \\ T_2 > R_2 & R_1 \leq \frac{T_m}{J_e}\cos\delta_{11} \leq R_2 \\ \frac{T_m}{J_e}\cos\delta_{11} < T_2 < R_1, T_2 > R_2 & R_1 > \frac{T_m}{J_e}\cos\delta_{11} \end{array}\right\} \tag{21}$$

(2) The stability of the equilibrium point A_2 is analyzed by substituting the value of the point A_2 into the determinant of the matrix $\boldsymbol{H}_1$.

$$\det\boldsymbol{H}_1\big|_{A_2} = \frac{K_Z}{J_m}T\cos\delta_{12} = -\frac{K_Z}{J_m}\sqrt{T^2 - \left(\frac{T_m}{J_e}\right)^2} < 0 \tag{22}$$

Since the Jacobian matrix of Equation (3) has a value of determinant less than 0 at the equilibrium point A_2, it has heteroscedasticity and the equilibrium point A_2 is unstable.

In summary: If the bifurcation parameter T satisfies $0 < T < T_m/J_e$, then there is no equilibrium point in Equation (3); if $T > T_m/J_e$, there exist two equilibrium points, A_1 and A_2, of the system, and the variant T_2 of T satisfies Equations (19) and (20), the system produces Hopf bifurcation at equilibrium point A_1. When T_2 satisfies Equation (21), equilibrium point A_1 is stable and equilibrium point A_2 is unstable; if $T = T_m/J_e$, equilibrium point A_1 coincides with equilibrium point A_2.

4. Stability Domain Analysis

The Lyapunov stability discriminant is a qualitative method that does not require solving complex differential equations of the system, but, rather, constructs a Lyapunov function and then directly determines the stability of the system based on the variation of the function over time. Therefore, it is suitable for calculating nonlinear systems that are difficult to solve [17].

The stability domain of the stable equilibrium position is estimated using Lyapunov's stability theorem. Shift the equilibrium point of Equation (3) to the origin of the coordinate axis.

$$\left.\begin{array}{l} u_1 = \hat{u}_1 + u_{11} \\ u_2 = \hat{u}_2 + u_{21} \\ \delta_1 = \hat{\delta}_1 + \delta_{11} \\ \delta_2 = \hat{\delta}_2 + \delta_{21} \end{array}\right\} \tag{23}$$

Equation (3) is transformed into the following form:

$$\left.\begin{array}{l} \frac{d\hat{u}_1}{dt} = \hat{u}_2 \\ \frac{d\hat{u}_2}{dt} = -\frac{K_Z}{J_m}\hat{u}_1 - \frac{(C_m+C_Z)}{J_m}\hat{u}_2 + \frac{K_Z}{J_m}\hat{\delta}_1 + \frac{C_Z}{J_m}\hat{\delta}_2 \\ \frac{d\hat{\delta}_1}{dt} = \hat{\delta}_2 \\ \frac{d\hat{\delta}_2}{dt} = \frac{K_Z}{J_e}\hat{u}_1 + \frac{C_Z}{J_e}\hat{u}_2 - \left(\frac{K_Z}{J_e} + T\cos\delta_{11}\right)\hat{\delta}_1 - \frac{(C_e+C_Z)}{J_e}\hat{\delta}_2 \\ \quad -T\left[\sin\left(\hat{\delta}_1 + \delta_{11}\right) - \sin\delta_{11} - \hat{\delta}_1\cos\delta_{11}\right] \end{array}\right\} \tag{24}$$

Simplify Equation (24) to the following matrix vector form:

$$\dot{\boldsymbol{x}} = \boldsymbol{J}_2\boldsymbol{x} + \boldsymbol{r} \tag{25}$$

In Equation (25):

$$\boldsymbol{x} = \left(\hat{u}_1, \hat{u}_2, \hat{\delta}_1, \hat{\delta}_2\right)^T; \boldsymbol{r} = (0, 0, 0, g)^T; \tag{26}$$

$$g = -T\left[\sin\left(\hat{\delta}_1 + \delta_{11}\right) - \sin\delta_{11} - \hat{\delta}_1\cos\delta_{11}\right] \tag{27}$$

Select a quadratic function

$$V(\boldsymbol{x}) = \boldsymbol{x}^T\boldsymbol{P}\boldsymbol{x} \tag{28}$$

According to Lyapunov's stability theorem, the matrix $\boldsymbol{P}$ in Equation (28) is positive definite and the derivative $L(\boldsymbol{x})$ of $V(\boldsymbol{x})$ with respect to time is less than zero.

$$L(\boldsymbol{x}) = \frac{dV}{dt} < 0 \tag{29}$$

Constructing Lyapunov matrix equations

$$\boldsymbol{P}\boldsymbol{J}_2 + \boldsymbol{J}_2^T\boldsymbol{P} = -\boldsymbol{E} \tag{30}$$

when the bifurcation parameter T satisfies Equation (21), the matrix composed of the linear part of Equation (25) has a feature root of the negative real part, and the Lyapunov matrix equation has a symmetrical positive definite matrix.

Calculate the value of $L(\boldsymbol{x})$:

$$\begin{aligned} L(\boldsymbol{x}) = \tfrac{dV}{dt} &= \left(\tfrac{d\boldsymbol{x}}{dt}\right)^T \boldsymbol{P}\boldsymbol{x} + \boldsymbol{x}^T \boldsymbol{P}\left(\tfrac{d\boldsymbol{x}}{dt}\right) \\ &= \boldsymbol{x}^T(-\boldsymbol{E})x + 2(\boldsymbol{x},\boldsymbol{r}) \le -\|\boldsymbol{x}\|^2 + 2\|\boldsymbol{x}\|\|\boldsymbol{P}\boldsymbol{r}\| \end{aligned} \tag{31}$$

Taylor expansion and simplification of the expression for matrix g:

$$\begin{aligned} \|\boldsymbol{P}\boldsymbol{r}\| \le D\|\boldsymbol{r}\| = D|g| = \tfrac{1}{2}DT|\sin\xi|\left|\hat{\delta}_1\right|^2 \le \\ \tfrac{1}{2}DT|\sin\xi|\left|\hat{\delta}_1\right|\|\boldsymbol{x}\| \end{aligned} \tag{32}$$

where ξ is a constant and satisfies $\xi \in \left(\delta_{11}, \hat{\delta}_1 + \delta_{11}\right)$. D is the maximum eigenvalue of the symmetric positive definite matrix $\boldsymbol{P}$. According to the trigonometric function definition $|\sin\xi \le 1|$, the substitution Equation (32) is further simplified:

$$\|\boldsymbol{P}\boldsymbol{r}\| \le \frac{1}{2}DT\left|\hat{\delta}_1\right|\|x\| \tag{33}$$

The simplified numerical expression to obtain $L(\boldsymbol{x})$ is as follows:

$$\frac{dV}{dt} \le -\|\boldsymbol{x}\|^2\left(1 - DT\left|\hat{\delta}_1\right|\right) \tag{34}$$

Therefore, when $\left|\hat{\delta}_1\right| < \frac{1}{DT}$, $\frac{dV}{dt} \le 0$ can be obtained.

Since $|\sin\xi| \le |\xi| \le |\delta_{11}| + \left|\hat{\delta}_1\right|$, replace $|\sin\xi|$ in Equation (32) with $|\delta_{11}| + \left|\hat{\delta}_1\right|$ and calculate. The resulting equation of inequality is as follows:

$$\|\boldsymbol{P}\boldsymbol{r}\| \le \frac{1}{2}DT\left(|\delta_{11}| + \left|\hat{\delta}_1\right|\right)\left|\hat{\delta}_1\right|\|\boldsymbol{x}\| \tag{35}$$

$$\frac{dV}{dt} \le -\|\boldsymbol{x}\|^2\left(1 - DT\left(|\delta_{11}| + \left|\hat{\delta}_1\right|\right)\left|\hat{\delta}_1\right|\right) \tag{36}$$

Therefore, when $\left|\hat{\delta}_1\right| < \frac{1}{2}\left(-|\delta_{11}| + \sqrt{|\delta_{11}|^2 + \frac{4}{DT}}\right)$, $\frac{dV}{dt} \le 0$ can be obtained.

The two resulting value ranges are summarized and unified, and the stability domain of $\left|\hat{\delta}_1\right|$ is calculated as:

$$U = \max\left(\frac{1}{DT}, \frac{1}{2}\left(-|\delta_{11}| + \sqrt{|\delta_{11}|^2 + \frac{4}{DT}}\right)\right) \tag{37}$$

when $\left|\hat{\delta}_1\right| < U$, it means that at least one of the above inequalities is met to make it valid, so that $\frac{dV}{dt} < 0$ can be obtained, and the system is stable.

5. Parametric Effect Analysis

From the Equation (1), it can be seen that in the torsional vibration model of the wind turbine shaft system, the stability of the system is affected by each design parameter at the same time, and the influence of each design parameter on the stability of the system is different, so when analyzing the stability of the system, it is necessary to use the single variable method to analyze the action of each design parameter on the control parameter one by one. Since the first and second order Hurwitz determinants of the system are positive, and the symbols of the third and fourth order Hurwitz determinants are the same, it is only necessary to analyze the design parameters of the torsional vibration equation of equation (1) and the root R_i of the unary quadratic equation about T_2.

The rotational inertia J_m of the wind wheel and the rotational inertia J_e of the generator rotor are set as variables, where the rotational inertia J_m of the wind wheel varies from 1.141×10^4 to 1.441×10^4 kg·m^2 and the rotational inertia J_e of the generator rotor varies

from 4.170×10^4 to 4.470×10^4 kg·m^2. The values of R_i are calculated for different rotational inertia in the variation range, and the results are shown in Figures 2 and 3: when the rotational inertia J_m of the wind wheel increases gradually in the range, R_i decreases slowly with the increase of J_m. When the rotational inertia of the generator rotor J_e increases gradually in the range, R_i increases significantly with the increase of J_e.

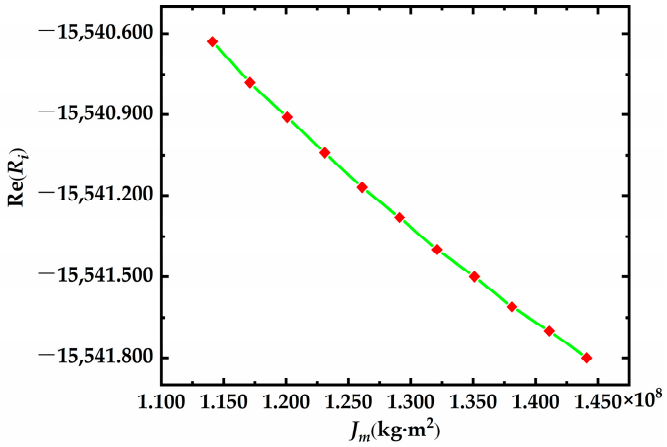

Figure 2. J_m results graph.

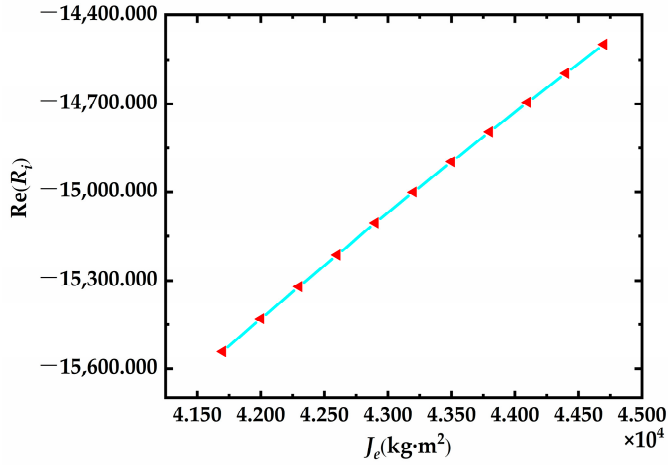

Figure 3. J_e results graph.

The damping coefficient C_m of the wind wheel, the damping coefficient C_z between the wind wheel and the generator, and the damping coefficient C_e of the generator rotor are set as variables, where the damping coefficient C_m of the wind wheel varies from 1.500 to 2.500 pu, the damping coefficient C_z between the wind wheel and the generator varies from 0.010 to 0.020 pu, and the damping coefficient C_e of the generator rotor varies from 0.500 to 1.500 pu. The values of R_i are calculated in the range of different damping coefficients, and the results are shown in Figures 4–6. When C_z and C_e gradually increase in the range, R_i gradually increases. When C_m increases gradually in the range, R_i decreases gradually.

The drive shaft stiffness coefficient K_z was set as a variable and varied from 6.526×10^8 to 6.826×10^8 N·m/rad. The value of R_i is calculated at different rotational inertia and the result is shown in Figure 7. R_i decreases as the stiffness coefficient K_z of the drive shaft increases in the range.

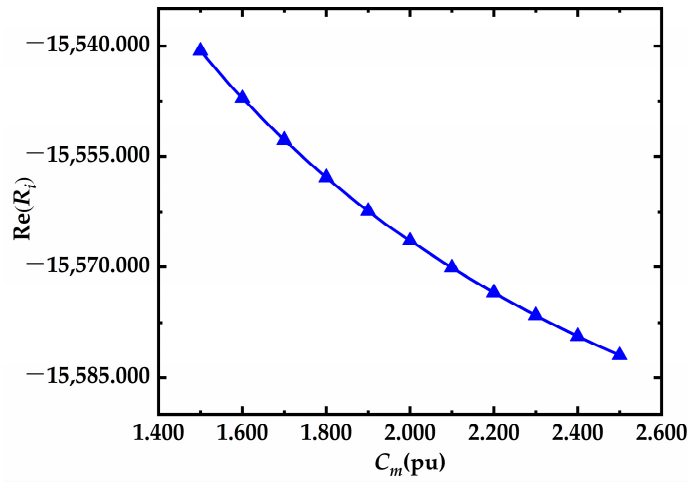

Figure 4. C_m results graph.

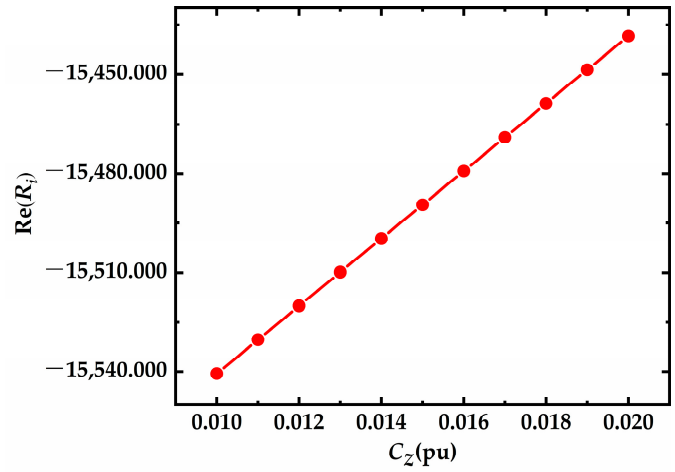

Figure 5. C_z results graph.

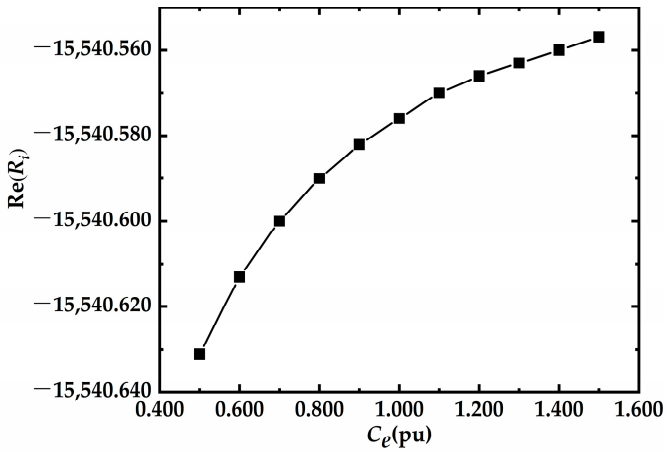

Figure 6. C_e results graph.

To quantitatively compare the magnitude of the effects of different design parameters on R_i over a range of variations, the paper introduces the sensitivity S as a measure. The sensitivity S is defined as follows [18]:

$$S = \frac{\Delta R/R}{\Delta x/x} \tag{38}$$

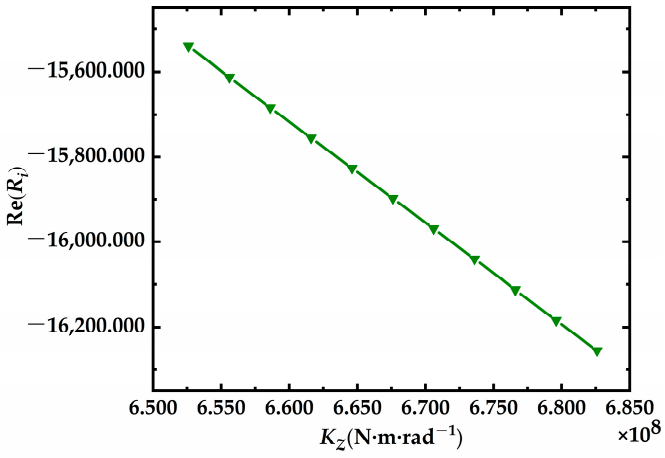

Figure 7. K_z results graph.

In Equation (38), ΔR is the value of R_i change for a certain design parameter change; x is the design parameter reference value; Δx is the design parameter change value.

From the definition of sensitivity, it is clear that the larger the value of S, the greater the influence of the analyzed design parameters on R_i. The design parameters were adjusted by +20% from the minimum of the range of values taken for the parametric effect analysis, and the degree of influence on R_i was analyzed by Equation (38), as shown in Table 3, and the degree of influence of each design parameter on R_i was ranked from largest to smallest as follows.

Table 3. Sensitivity of each parameter.

Parameters	Sensitivity
K_z	1.0000
J_e	0.8336
C_z	0.0066
C_m	0.0055
J_m	0.0003
C_e	5.9151×10^{-6}

It can be seen that K_z has the greatest influence, followed by J_e, C_z and C_m have less influence, while J_m and C_e has almost no influence. Combined with the actual engineering practice, when the value of sensitivity is set less than 0.1, the degree of influence of the parameters on the system is negligible. Therefore, the value of R_i can be adjusted by adjusting the value of K_z or J_e to achieve the control of system stability. When the value of R_i needs to be increased, the value of J_e can be adjusted to increase or the value of K_z can be adjusted to decrease, where the value of K_z is more effective. The opposite is also true.

6. Verification and Analysis

A model of wind turbine data is substituted into the torsional vibration system to calculate the range of values of the control parameters when the system is stable, and any value within the range is selected to calculate and verify whether the Routh–Hurwitz stability criterion is satisfied.

The values of each parameter are shown in the following Table 4:

Table 4. Table of values for each parameter.

Parameter	Value
J_m	1.141×10^8 kg·m^2
J_e	4.170×10^4 kg·m^2
K_z	6.526×10^8 N·m/rad
C_m	1.500 pu
C_e	0.500 pu
C_z	0.010 pu
T_m	4.524×10^5 N·m

Substituting the values of the parameters in Table 4 into Equations (10) and (16), the fixed values T_m/J_e and the two roots R_1 and R_2 are calculated.

$$T_m/J_e = 10.8489$$

$$R_1 = -15540.631 - 9104.354\,i,\ R_2 = -15540.631 + 9104.354\,i$$

According to Equation (21), since the real parts of the two roots of the unary quadratic polynomial R_1 and R_2 are less than the fixed values T_m/J_e, when T_2 is greater than $(T_m/J_e)\cos\delta_{11}$, that is, $T > 10.8489$, the system is stable at the equilibrium point A_1, and the Hopf bifurcation phenomenon is not generated. The stable range is (10.8489, $+\infty$).

Verify the correctness of the value range, and take the parameter value range $T = 123$ for stability analysis.

When $T = 123$, the Jacobian matrix at equilibrium point A_1 is:

$$\boldsymbol{H}_2 = \begin{bmatrix} 0 & 0.0001 & 0 & 0 \\ -0.0006 & -0.0000 & 0.0006 & 0.0000 \\ 0 & 0 & 0 & 0.0001 \\ 1.5650 & 0.0000 & -1.5772 & -0.0000 \end{bmatrix} \times 10^4$$

Eigenvalut1e:

$$\lambda_{1,2} = -6.1130 \times 10^{-6} \pm 125.6100\,i,\ \lambda_{3,4} = -8.7272 \times 10^{-9} \pm 0.2108\,i$$

According to Routh–Hurwitz theory, when $T = 123$, the eigen equation has an eigen root with a negative real part, and the system is stable at the equilibrium point A_1.

$$\delta_{11} = 0.0883 + 2k\pi,\ A_1 = (0.0890 + 2k\pi, 0, 0.0883 + 2k\pi, 0)$$

The positive definite matrix $\boldsymbol{P}$ is obtained as follows:

$$\boldsymbol{P} = \begin{bmatrix} 0.6942 & 0.0000 & -0.6398 & 0.0000 \\ 0.0000 & 1.3359 & 0.0000 & 0.0004 \\ -0.6398 & 0.0000 & 0.6448 & 0.0000 \\ 0.0000 & 0.0004 & 0.0000 & 0.0000 \end{bmatrix} \times 10^9$$

The four eigenvalues of the positive definite matrix $\boldsymbol{P}$ are calculated to be 40,900, 2.9230×10^7, 1.3100×10^9, and 1.3359×10^9. The maximum eigenvalue D is 1.3359×10^9. Further derive the two stable domains $U_1 = 6.0858 \times 10^{-12}$ and $U_2 = 6.8371 \times 10^{-11}$ of δ in the system. The stability domain δ at equilibrium point A_1 is $\left|\hat{\delta}_1\right| < 6.8371 \times 10^{-11}$.

7. Conclusions

A torsional vibration model of the shaft system of a direct-drive permanent magnet wind turbine was established, and the Jacobian matrix of the equilibrium point of the torsional vibration model was analyzed to obtain the stability of the torsional vibration

system and the range of the control parameters when the bifurcation phenomenon occurred by using the Routh–Hurwitz stability criterion.

By constructing the Lyapunov function, the range of the stable domain of the equilibrium position in the steady state of the torsional vibration system was obtained. The sensitivity analysis of the system parameters was performed to obtain the effects of the system parameters on the stability of the system for torsional vibration systems.

The bifurcation and stability calculation of the shaft system torsional vibration of a type of direct-drive wind wheel was a research object. The results show that the method proposed in the paper can be used for bifurcation and stability domain analysis of torsional vibration of wind wheel shaft systems.

In this article, we obtained the range of values of control parameters for the stability of torsional vibration systems and the bifurcation phenomenon, and, in the subsequent work, we can analyze the characteristics of the system when the bifurcation phenomenon occurs at the equilibrium point and how to control it.

Author Contributions: Conceptualization, Z.H., R.W. and J.C.; methodology, Z.H. and R.W.; software, R.W., J.C., X.X. and Y.X.; validation, Z.H., R.W. and J.C.; formal analysis, Z.H., R.W. and J.C.; investigation, J.C. and X.X.; resources, Z.H.; data curation, R.W. and J.C.; writing—original draft preparation, Z.H., R.W. and J.C.; writing—review and editing, Z.H., R.W., J.C. and X.X.; visualization, Z.H., R.W. and J.C.; supervision, Z.H., X.X. and Y.X.; project administration, Z.H. and R.W.; and funding acquisition, Z.H. All authors have read and agreed to the published version of the manuscript.

Funding: This research was funded by the Project of National Natural Science Foundation of China [51875193], and the Project of scientific foundation of Hunan provincial education department [21B0668].

Data Availability Statement: All data used to support the findings of this study are included within the article.

Conflicts of Interest: The authors declare no conflict of interest.

References

1. Pourbeik, P.; Sanchez-Gasca, J.; Senthil, J.; Weber, J.; Zadehkhost, P.; Kazachkov, Y.; Tacke, S.; Wen, J.; Ellis, A. Generic Dynamic Models for Modeling Wind Power Plants and Other Renewable Technologies in Large-Scale Power System Studies. *J. IEEE Trans. Energy Convers.* **2017**, *32*, 1108–1116. [CrossRef]
2. Zeng, Y. The "14th Five-Year Plan" period of China's renewable energy development will enter a new phase. *Nat. Gas Oil* **2021**, *39*, 112.
3. Gao, B.; Cui, Y.; Shao, B.; Liu, Y.; Zhao, S. Analysis of sub-synchronous oscillation characteristics of direct-drive wind turbines in the full operation region. *Electr. Power Construct.* **2020**, *41*, 85–93.
4. Zhou, P.; Song, R.; Li, G.; Du, N.; Chang, X.; Guo, X. Direct-drive wind turbine sub-synchronous oscillation damping control method and its adaptability. *Autom. Electr. Power Syst.* **2019**, *43*, 177–184.
5. Gao, Z.; Liu, X. An Overview on Fault Diagnosis, Prognosis and Resilient Control for Wind Turbine Systems. *Processes* **2021**, *9*, 300. [CrossRef]
6. Fu, Y.; Gao, Z.; Liu, Y.; Zhang, A.; Yin, X. Actuator and Sensor Fault Classification for Wind Turbine Systems Based on Fast Fourier Transform and Uncorrelated Multi-Linear Principal Component Analysis Techniques. *Processes* **2020**, *8*, 1066. [CrossRef]
7. Sun, S.; Huo, Q.; Sun, L.; Guo, L.; Wang, R.; Kong, X. Analysis of torsional vibration mechanism and suppression strategy of double-fed wind turbine shaft system considering whole machine torque control. *Electr. Power* **2022**, *55*, 39–46.
8. Wang, Z.; Li, X. Nonlinear Control of Torsional Vibration of Direct Drive Permanent Magnet Wind Turbine Shaft System. *J. Wuhan Inst. Technol.* **2018**, *40*, 93–97.
9. Saenz-Aguirre, A.; Zulueta, E.; Fernandez-Gamiz, U.; Teso-Fz-Betoo, D.; Olarte, J. Kharitonov theorem based robust stability analysis of a wind turbine pitch control system. *J. Math.* **2020**, *8*, 964. [CrossRef]
10. Agarala, A.; Bhat, S.; Mitra, A.; Zychma, D.; Sowa, P. Transient Stability Analysis of a Multi-Machine Power System Integrated with Renewables. *J. Energies* **2022**, *15*, 4824. [CrossRef]
11. Siddiqui, M.; Khalid, M.; Badar, A.; Saeed, M.; Asim, T. Parametric Analysis Using CFD to Study the Impact of Geometric and Numerical Modeling on the Performance of a Small Scale Horizontal Axis Wind Turbine. *J. Energies* **2022**, *15*, 505. [CrossRef]
12. Ubando, T.; San, R.; Cruz, P. Savonius Wind Turbine Numerical Parametric Analysis Using Space-Filling Design and Gaussian Stochastic Process. *J. Wind* **2022**, *2*, 113–128. [CrossRef]
13. Shrestha, A.; Gonzalez-Longatt, F. Parametric sensitivity analysis of rotor angle stability indicators. *J. Energies* **2021**, *14*, 5023. [CrossRef]

14. Moghadam, K.; Nejad, R. Theoretical and experimental study of wind turbine drivetrain fault diagnosis by using torsional vibrations and modal estimation. *J. Sound Vib.* **2021**, *509*, 116223. [CrossRef]
15. Jie, D.; Wang, R.; Wang, X.; Zhang, Y. Model and mechanism of torsional vibration of multi-model wind turbine network. *Acta Energy Sol. Sin.* **2011**, *32*, 1281–1287.
16. Jing, Z.; Wang, J. Torsional vibration bifurcation analysis and stability domain estimation of turbine-generator shaft system. *Autom. Electr. Power Syst.* **2001**, *4*, 6–10.
17. Qin, H.; Ding, B.; Tan, J. Constructing Lyapunov functions to determine the stability of ordinary differential equations. *J. Chongqing Univ. Technol. Nat. Sci.* **2005**, *19*, 139–141.
18. Zaaijer, M. Foundation Modelling to Assess Dynamic Behavior of Offshore Wind Turbines. *Appl. Ocean Res.* **2006**, *28*, 45–57. [CrossRef]